Electrically-assisted lasing in metal halide perovskite semiconductors

Alex J. Grede,*,†,‡ Robert Cawthorn,†,¶ Lianfeng Zhao, $\S, \|$ John P. Murphy,†,‡ Kwangdong Roh, \S, \bot Khaled Al Kurdi,# Stephen Barlow,#, @ Seth R. Marder, $\#, @, \triangle$ Barry P. Rand, \S, ∇ and Noel C. Giebink*,†,¶

†Department of Electrical Engineering, The Pennsylvania State University, University

Park, Pennsylvania 14802, United States

‡NRC Postdoc residing at the U.S. Naval Research Laboratory, Washington D.C., 20375,
United States

- ¶Department of Electrical Engineering and Computer Science, University of Michigan,
 Ann Arbor, Michigan 48109, United States
- §Department of Electrical and Computer Engineering, Princeton University, Princeton,

 New Jersey 08544, United States
- || Holcombe Department of Electrical and Computer Engineering, Clemson University,
 | Clemson, South Carolina 29634, United States
- ⊥Department of Physics, Ewha Womans University, Seoul 03760, Republic of Korea

 #School of Chemistry and Biochemistry and Center for Organic Photonics and Electronics,

 Georgia Institute of Technology, Atlanta, GA 30303, United States
- @Renewable and Sustainable Energy Institute (RASEI), University of Colorado Boulder,
 Boulder, Colorado 80309, United States
 - $\triangle Department$ of Chemistry and Department of Chemical and Biological Engineering,

 University of Colorado Boulder, Boulder, Colorado 80309, United States $\nabla And linger$ Center for Energy and the Environment, Princeton University, Princeton,

E-mail: agrede@ieee.org; ngiebink@umich.edu 2

New Jersey 08544, United States

Abstract

Metal halide perovskite (MHP) semiconductors offer the prospect of wavelength-tunable diode lasers fabricated on a wide range of substrates without lattice matching concerns. However, all MHP lasers to date are optically pumped. Here, we show that electrically-injected carriers can assist lasing in a MHP composition of formamidinium lead iodide and methylammonium lead bromide ((FAPbI₃)_{0.95}(MAPbBr₃)_{0.05}) under short, high current electrical pulses at low temperature. Using a distributed feedback resonator, doped organic transport layers, and a custom impulse circuit that delivers electrical pulses as short as 3 ns, we are able to inject a carrier density of approximately 6×10^{17} cm⁻³ at T = 230 K and show that it leads to a ~24% reduction in the optically-pumped lasing threshold when the optical pulse overlaps the first few ns of the electrical pulse. These results support the viability of MHP laser diodes and indicate that roughly an order of magnitude reduction in threshold carrier density will be required to achieve pure electrically-pumped lasing in (FAPbI₃)_{0.95}(MAPbBr₃)_{0.05} at low temperature.

Keywords

MHP, diode laser, non-epitaxial, thin film, stimulated emission

Metal halide perovskite semiconductors are a promising platform to realize a nonepitaxial laser diode because they are efficient light emitters with a tunable bandgap that can be solution-processed on a wide range of substrates. They have demonstrated low threshold optically-pumped lasing, ^{2–4} light-emitting diodes (LEDs) that operate under high current injection, ^{5–8} LEDs that lase under optical pumping and, very recently, electrically-assisted amplified spontaneous emission (ASE) from LEDs under combined optical and electrical excitation. This last milestone by Elkhouly et al. is especially significant because it shows that injecting 3 kA cm⁻² can reduce the optically-pumped ASE threshold by about 13%, which establishes the remaining improvement that will be required to achieve stimulated emission under pure electrical pumping.

Here, we take an important next step by fabricating a full distributed feedback (DFB) perovskite laser diode and demonstrating that it achieves electrically-assisted lasing under short, high current pulsing at low temperature. The device architecture employs a mixed formamidinium lead iodide and methylammonium lead bromide $((\text{FAPbI}_3)_{0.95}(\text{MAPbBr}_3)_{0.05})$ active layer with a 2^{nd} order SiO_2 DFB grating and doped organic transport layers to reduce series resistance. Using a custom impulse circuit, we are able to inject an estimated carrier density of $6 \times 10^{17} \, \text{cm}^{-3}$ during 20 ns electrical pulses, which amounts to roughly one quarter of the optical threshold at 230 K. Under these conditions, we observe a $\sim 24\%$ decrease in the optically-pumped laser threshold when the optical pulse overlaps the first few ns of the electrical pulse. These results indicate that roughly an order of magnitude reduction in the threshold carrier density will be required to achieve pure electrically-pumped lasing in $(\text{FAPbI}_3)_{0.95}(\text{MAPbBr}_3)_{0.05}$ at low temperature.

Figure 1(a) illustrates the device architecture, which consists of an 80 nm-thick SiO₂ grating patterned via e-beam lithography on indium-tin-oxide (ITO; 120 nm thickness with a sheet resistance of $15\,\Omega/\Box$)-coated glass. The grating period is $\Lambda=410\,\mathrm{nm}$ and its $f\sim0.3$ duty cycle is optimized to reduce the threshold gain via rigorous coupled wave analysis (RCWA) simulations described in the Supplementary Material. The hole transport

layer (HTL) consists of poly(2,4,6-trimethyltriphenylamine-4',4"-diyl) (PTAA) p-doped with 2,3,5,6-tetrafluoro-7,7,8,8-tetracyanoquinodimethane (F₄TCNQ). ¹⁰ The HTL is spin-coated at a nominal thickness of 20 nm on a flat reference wafer; however, the actual thickness between the grating ridges in Fig. 1(b) is likely thicker.

The subsequent $(FAPbI_3)_{0.95}(MAPbBr_3)_{0.05}$ layer is also spin-coated and planarizes the grating with a thickness of approximately 140 nm between the ridges (Fig. 1(b)). It is important to note, however, that the thickness of the $(FAPbI_3)_{0.95}(MAPbBr_3)_{0.05}$ layer varies by ~ 20 nm over the $15 \,\mu\text{m} \times 100 \,\mu\text{m}$ active device area windowed in the SiO_2 . Accounting for this thickness variation is important to correctly tune the resonant mode of the grating to the peak of the $(FAPbI_3)_{0.95}(MAPbBr_3)_{0.05}$ gain spectrum. The $(FAPbI_3)_{0.95}(MAPbBr_3)_{0.05}$ layer is followed by a $40 \,\mu\text{m}$ -thick electron transport layer (ETL) consisting of 2,4,6-tris (3-(diphenyl phosphoryl)) triazine (PO-T2T) co-evaporated with the n-dopant (pen-tamethylcyclopentadienyl) (1,3,5-trimethylbenzene)ruthenium dimer $([RuCp^*Mes]_2)$. The stack is completed with a $100 \,\mu\text{m}$ -thick Ag cathode, and a graphite heat spreader is subsequently added on top of the device, similar to Zhao et al. 5 .

The devices are characterized in a continuous flow liquid N_2 cryostat using a home-built microscope equipped with a long working distance objective as shown in Fig. 1(c). The entire system mounted to three motorized linear stages to control position and focus. High voltage electrical pulses with controllable duration in the range <1 to 100 ns are generated using the impulse circuit described in the Supplementary Material. The pulses are delivered via mini-coax cables and a custom printed circuit board connector with 50 Ω transmission lines that terminate on the anode of each device through pogo pins that press the substrate against the cryostat cold head (Fig. 1(c)). Optical excitation pulses ($\lambda = 532 \, \text{nm}$, 22 ps duration) are focused through the microscope to a \sim 50 μ m-wide stripe that overlaps the device active area as shown in Fig. 1(c). Emission is collected exclusively from a small spot at the center of the device active area using a 50 μ m multimode fiber optic cable connected to a streak camera that is synced to both the optical and electrical pulses using a digital

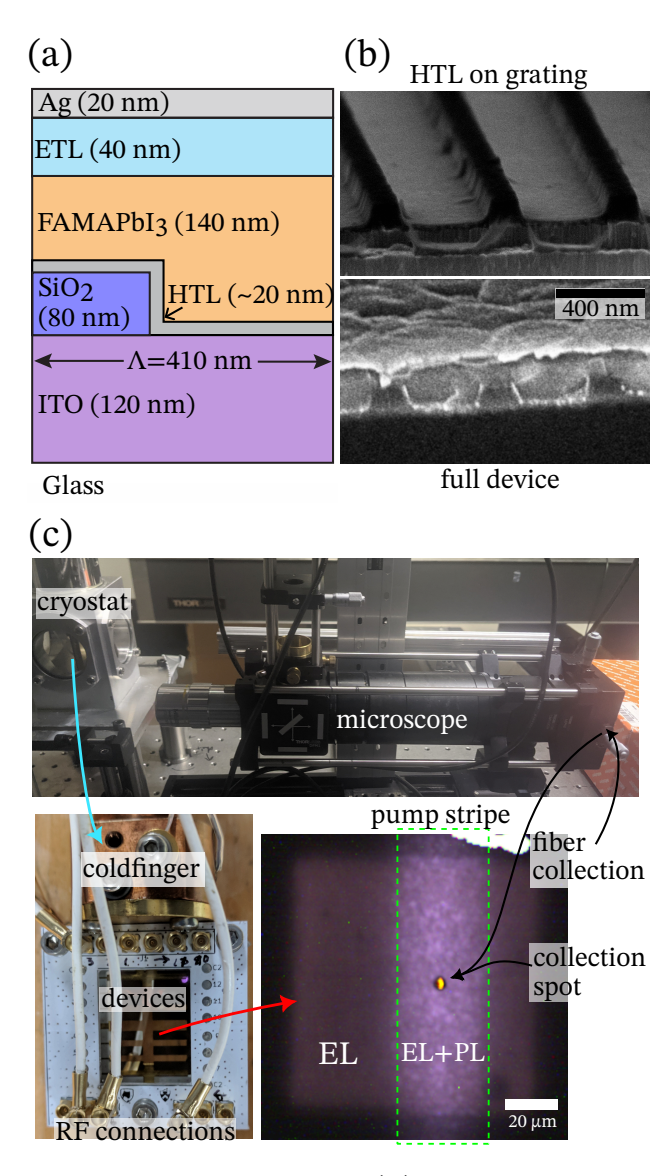


Figure 1: (a) Schematic of the device architecture. (b) Cross-sectional SEM images of the grating after deposition of the HTL (upper), and the completed device stack (lower). (c) The experimental setup consists of a horizontal epifluorescent microscope focused on devices mounted in a cryostat with $50\,\Omega$ connections located as close to the device as possible. Devices ($100\,\mu\text{m} \times 100\,\mu\text{m}$ active area shown in the lower right image) are pumped with a pulsed laser focused to a stripe (dashed green box). Emission (both electroluminescence and photoluminescence) is collected confocally from a small spot in the center of the pump stripe (orange spot) into a multimode fiber that can be connected to a streak camera or a cooled CCD spectrograph.

delay generator. Time-averaged emission spectra are recorded by plugging the collection fiber into a cooled CCD grating spectrometer. Full details on the electrical interconnection and timing scheme are provided in the Supplementary Material.

Figure 2(a) shows a series of optically-pumped emission spectra measured at fluences below, at, and above laser threshold for a typical 100 µm × 100 µm square device at T = 230 K. Stimulated emission is isolated in each case by fitting a Gaussian to the background photoluminescence (PL) and subtracting it from the data, similar to Elkhouly et al. ⁹. Integrating the result yields the threshold curve for stimulated emission plotted in Fig. 2(b). The top axis of Fig. 2(b) provides an upper bound estimate of the excited carrier density assuming the pump is fully absorbed in the (FAPbI₃)_{0.95}(MAPbBr₃)_{0.05} active layer, which yields a threshold of $n_{\text{th,opt}} \approx 2 \times 10^{18} \text{ cm}^{-3}$ under optical-only excitation.

Figure 2(c) establishes the maximum carrier density that can be electrically injected, in this case for a rectangular $15 \,\mu\text{m} \times 100 \,\mu\text{m}$ device, by comparing the transient electroluminescence (EL) intensity from a $20 \, \text{ns}$, $21 \, \text{V}$ pulse (as measured by a voltage monitor from the output of the pulsing circuit) with the transient PL intensity under optical excitation (of the same device under identical detection conditions) just below threshold. Since the instrument response function (IRF; gray line) is fast enough to capture the instantaneous peak of the PL, and the radiative recombination rate is proportional to the square of the carrier density under high-level injection, ¹¹ the $15 \times$ difference between the peak PL and EL intensities in Fig. 2(c) implies that electrical injection in this device delivers about $25 \,\%$ of the optically-pumped threshold carrier density insofar as local current variation due to the SiO₂ grating ridges can be neglected.

While this level of electrical injection is not sufficient to achieve lasing by itself, it does yield a measurable assist under combined optical+electrical co-pumping as shown in Fig. 3. In this case, the optical pulse fluence is set just below threshold and timed to reach the sample 1 ns before or after the start of the electrical pulse (Fig. 3(a), inset). The associated spectra in Fig. 3(a) show that this 2 ns timing difference has little effect on the background EL+PL

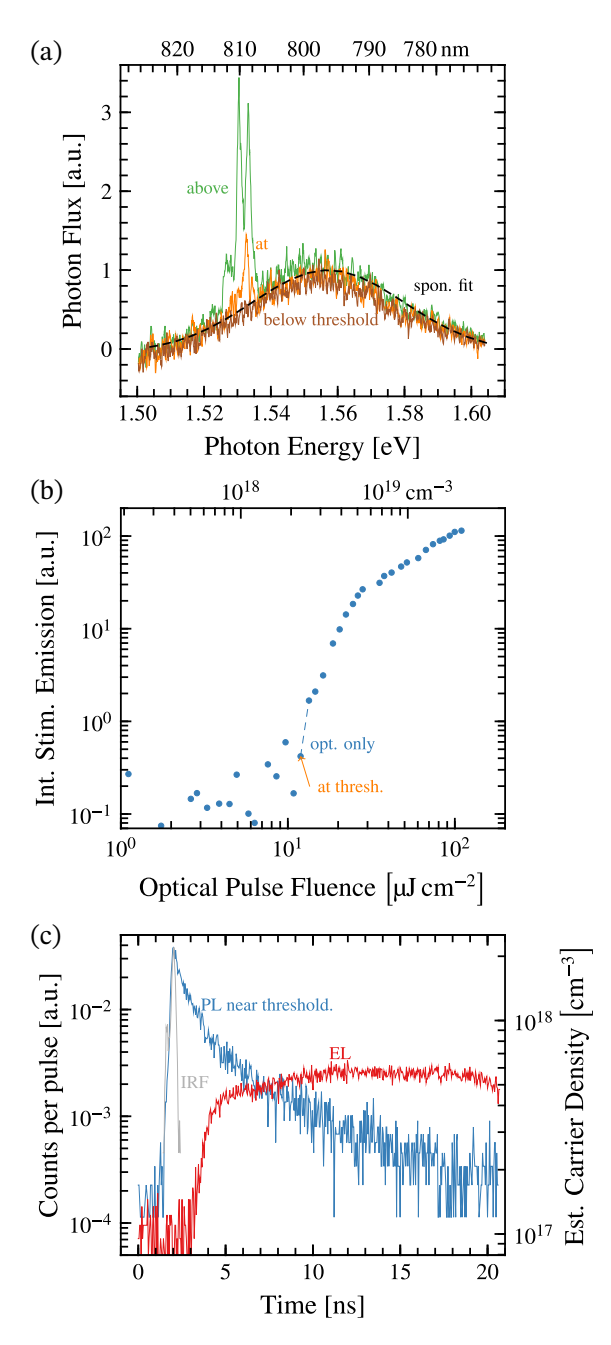


Figure 2: (a) Optically-pumped emission spectra collected at pulse fluences slightly below, at, and above laser threshold. The black dashed line is an example Gaussian fit to the spontaneous emission background of the above threshold spectrum (green). The substructure in the emission line above threshold likely originates from etaloning by the edges of the SiO₂ window that defines the device active area. (b) Integrated intensity at the laser line after subtracting the spontaneous emission background in (a). The top axis shows the calculated carrier density assuming that the pump pulse is fully absorbed by the 140 nm-thick (FAPbI₃)_{0.95}(MAPbBr₃)_{0.05} active layer. (c) Streak camera PL and EL transients collected separately from the same device under identical measurement conditions. The PL transient is excited with an optical pulse fluence just below threshold and serves as a reference point for the electrically-injected carrier density that is reached during the 21 V (at the voltage monitor), 20 ns EL pulse.

spontaneous emission, but has a significant effect on emission at the laser line, implying that the electrical pulse boosts the device above threshold. Figure 3(b) shows the threshold characteristic acquired for each timing sequence, which confirms that coincident co-pumping reduces the threshold optical pulse fluence by about 24% relative to the non-overlapped case. The magnitude of the threshold reduction is smaller (about 10%) when compared to the optical-only measurement in Fig. 2(b) because the latter does not include accumulated heating from the electrical pulse train that increases the threshold carrier density. Since the optical-before-electrical co-pumping case does account for this, it represents the more meaningful reference point.

Crucially, Fig. 4(a) shows that the lasing assist in Fig. 3 only occurs within the first few ns of the electrical pulse. When the optical pulse arrives 10 ns into the electrical pulse, emission at the laser line is quenched, presumably due to the buildup of heat. The fact that a few ns timing difference separates assistance from quenching indicates that these observations are not related to field-induced ion migration, which alters laser threshold on a much longer timescale (i.e., commensurate with the time average of the electrical pulse train). ¹³

The dependence of the lasing assist on electrical pulse amplitude for an optimally-delayed optical pulse is more nuanced (Fig. 4(b)). Although the stimulated emission signal is enhanced on average relative to optical-only pumping over the 30 to 50 V range, the signal is volatile. Neither the volatility nor the absence of lasing above 52 V is due to device degradation, as both were repeatably cycled between different voltages and each data point represents the average over more than 200 electrical pulses. The spontaneous emission background, by contrast, displays a steady decrease with increasing voltage, which suggests that higher pulse amplitude actually reduces the total rate of radiative recombination, likely due to heating. Taken together with the behavior in Fig. 4(b), the message is that letting heat accumulate for too long, 12 or generating it too fast (at a rate $\propto V^2$) quickly overwhelms the ability to assist lasing.

In this context, it is worth discussing and justifying the pulsing conditions and choice of

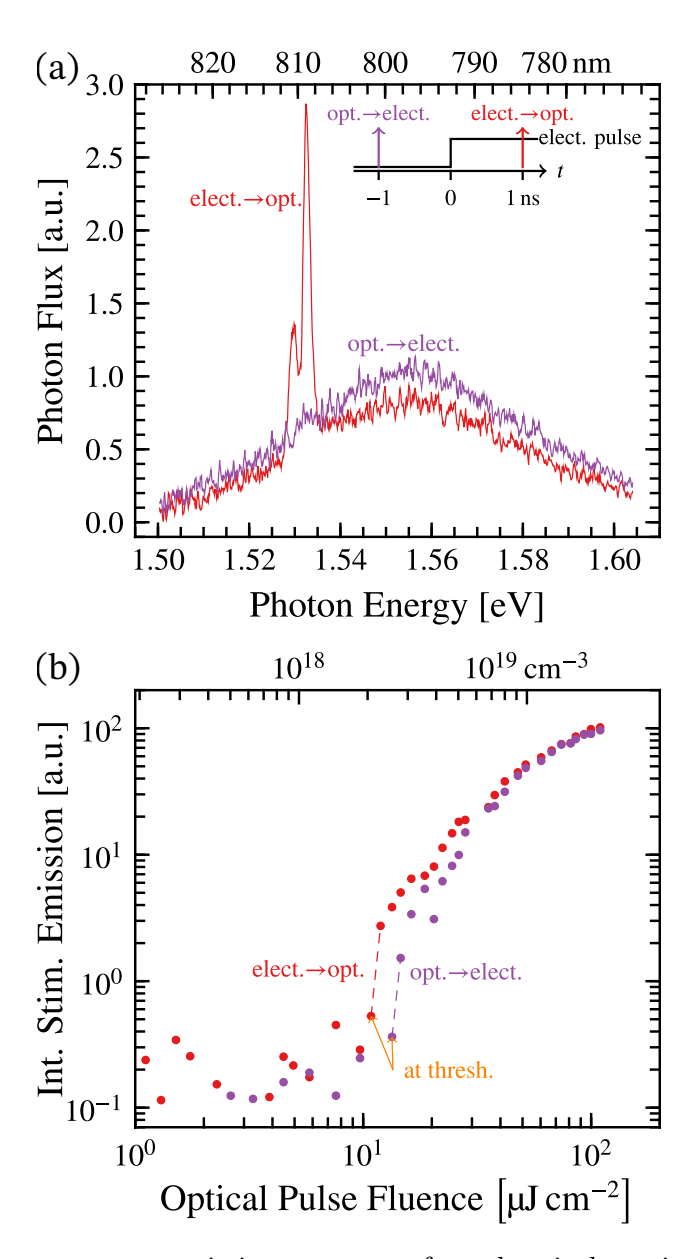


Figure 3: (a) Time-average emission spectra for electrical+optical co-pumping of a $100 \,\mu\text{m} \times 100 \,\mu\text{m}$ square device at $T = 230 \,\text{K}$. The optical pulse fluence is set to $90 \,\%$ of threshold and timed to arrive just before (opt. \rightarrow elect.) or just after (elect. \rightarrow opt.) the electrical pulse as depicted in the inset. The electrical pulse amplitude is $52 \,\text{V}$. (b) Full input-output characteristics recorded for each timing sequence as a function of optical pulse fluence. The optical contribution to the carrier density is shown on the top axis assuming the optical pulse is fully absorbed in the $(\text{FAPbI}_3)_{0.95}(\text{MAPbBr}_3)_{0.05}$ layer.

 $T=230\,\mathrm{K}$ as the measurement temperature. The latter was chosen because it is the lowest temperature (and thus lowest threshold carrier density; see Supplementary Fig. S2) at which we could maximize electrical injection without irreversibly damaging the devices. Since the device impedance is a strong function of temperature, it is difficult to match to the pulsing circuit *a priori*. Therefore, at the beginning of an experiment, one of the devices on the substrate was typically sacrificed to determine the maximum electrical pulse amplitude that could be tolerated without causing irreversible degradation.

The temperature-dependent impedance mismatch also makes it difficult to accurately determine both the voltage and current at the device because a portion of the electrical pulse is reflected. Figure 4(a) provides a measurement of the voltage and a calculation of the current derived from the voltage monitor output of the pulsing circuit. However, the pulses are short enough that there is an appreciable time lag between the voltage and current leaving the pulser, and each quantity at the device. This issue arises for any high speed pulsing measurement where the voltage and current are not probed near the device. The integrated measurement resistor described by Chime et al. ¹⁴ could resolve this issue, but was not straightforward to implement in these particular devices. Consequently, we rely on the PL-calibrated EL intensity from Fig. 2(c) as the best measure of injected carrier density in this work.

Looking ahead to the ultimate goal of pure electrically-pumped lasing, there are several near-term opportunities to improve the device architecture. Better impedance matching, the addition of an integrated measurement resistor (to simplify current measurement), and redesign of the DFB resonator to eliminate the electrical dead spots that currently exist above the SiO_2 grating ridges would all help to increase the gain. However, it seems clear from Fig. 4(b) that simply injecting more current without also addressing heat dissipation (e.g., by reducing series resistance in the device) is counterproductive, particularly since Fig. 4(a) implies that heat buildup becomes problematic within just a few ns. To this point, we tried a series of co-pumping measurements on $(FAPbI_3)_{0.95}(MAPbBr_3)_{0.05}$ LEDs with electrical

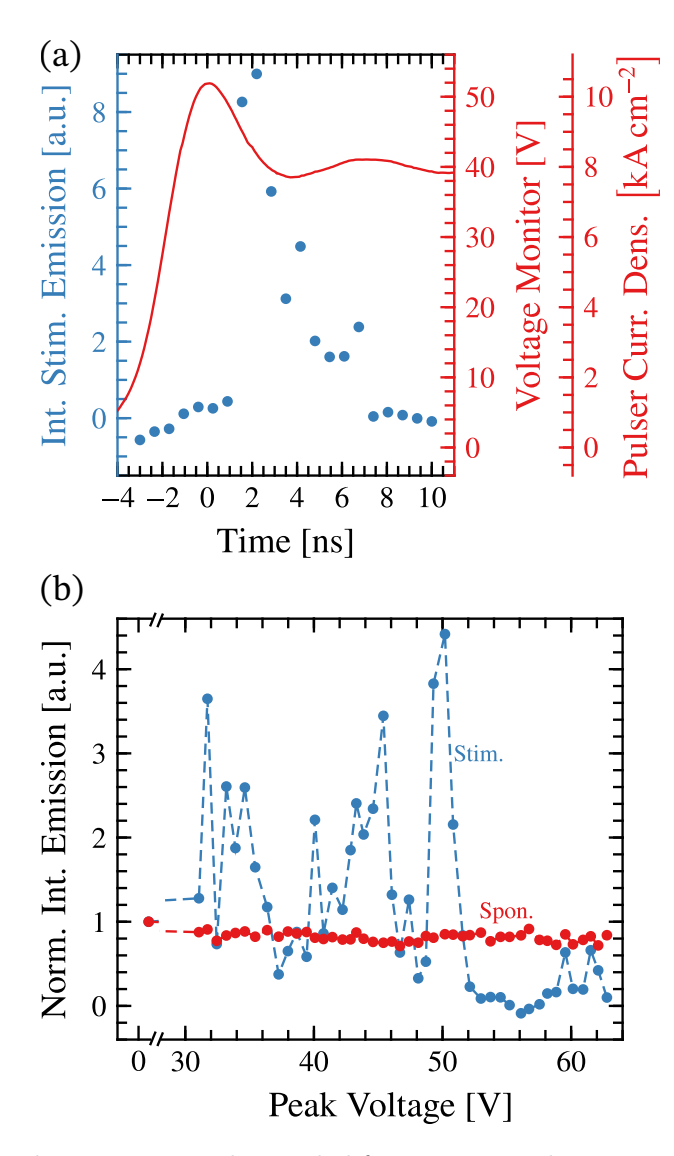


Figure 4: (a) Stimulated emission signal recorded from a square device in a co-pumping experiment similar to that in Fig. 3, but with varying optical pulse delay. The lasing assist peaks and then disappears over the first few ns of the electrical pulse. When the optical pulse arrives more than ~ 8 ns into the electrical pulse, no lasing is observed. The red trace shows the voltage monitor from the impulse circuit together with the pulser current density calculated by dividing the voltage monitor by a $50\,\Omega$ load and normalized to the area of the device (right-hand axes). The rise time of the red trace is limited by the $100\,\mathrm{MHz}$ bandwidth of the oscilloscope used to measure it. (b) Stimulated emission signal recorded from a rectangular device as a function of pulse voltage at an optimal electrical—optical pulse delay of $0.7\,\mathrm{ns}$. No lasing is observed for pulse amplitudes higher than $\sim 52\,\mathrm{V}$.

pulse widths of just 3 ns, but were unable to achieve an assist for amplified spontaneous emission; see the Supplementary Material for details.

The overwhelming priority, therefore, is to reduce the threshold carrier density, by approximately an order of magnitude, to $n_{\rm th} \sim 10^{17}\,{\rm cm}^{-3}$. This has been achieved in optically-pumped halide perovskite lasers ^{15–17} but not, to our knowledge, in a diode laser architecture. Possibilities to help reach this goal include adopting a mixed order grating ¹⁸ or a low loss ring resonator architecture, hot-pressing or nanoimprinting the perovskite to reduce its surface roughness-induced scattering loss, ¹⁷ and replacing the top Ag contact with a lower loss transparent conducting oxide as in Elkhouly et al. ⁹. Finally, 140 nm of (FAPbI₃)_{0.95}(MAPbBr₃)_{0.05} is simply a large amount of material to invert. Confining recombination to a smaller volume of active layer material (e.g., small, lower band gap inclusions in a mixed phase perovskite ²) in the same spirit as III-V quantum well lasers would be beneficial, but only after the dominant extrinsic optical losses above have been eliminated.

In summary, we have shown that electrically-injected carriers can assist lasing in $(FAPbI_3)_{0.95}(MAPbBr_3)_{0.05}$ under short, high current electrical pulsing at low temperature. This result reinforces recent observations of electrically-assisted ASE, ⁹ adding momentum to the worldwide effort to realize a perovskite laser diode. By systematically increasing the electrical assist fraction through reduction of the threshold carrier density, this goal finally appears to be within reach.

Methods

Materials. Formamidium iodide (FAI), methylammonium bromide (MABr), and methylammonium chloride (MACl) were purchased from Greatcell Solar Materials. PbI₂ and PbBr₂ were purchased from Tokyo Chemical Industry (TCI). PTAA was purchased from Solaris Chem. PO-T2T was purchased from Xi'an Polymer Light Technology. F₄TCNQ was purchased from Ossila. [RuCp*Mes]₂ was synthesized as described elsewhere. ¹⁹ Dimethyl-

formamide (DMF), dimethyl sulfoxide (DMSO) and chlorobenzene were purchased from Sigma-Aldrich. The graphite sheet $(50\,\mu\text{m})$ with an insulating adhesive layer $(6\,\mu\text{m})$ was manufactured by Panasonic. All materials were used as received.

Device Patterning and Grating Fabrication. The device layout design is similar to our previous work.⁵ A narrow ITO anode strip with a width of 200 µm is patterned by a wet etching process. Then, a patterned Au layer (200 nm, deposited by electron-beam evaporation) connected to the ITO strip is formed by a lift-off process to reduce series resistance. A thin film of SiO_2 was grown by PECVD at 70 °C on top of the ITO and Au layers. To form both the DFB grating and device active area, the SiO_2 films were patterned and completely etched using electron-beam lithography (50 nm of PMMA was used as a resist layer, followed by development at -20 °C to enhance resolution) and an inductively coupled plasma etching process. The device active area is defined by the windowed region in the SiO_2 containing the DFB grating, which is smaller than the area of the overlap between the bottom ITO anode strip and the top Ag cathode strip.

Perovskite Device Fabrication. The perovskite precursor solution was prepared in an N_2 -filled glovebox that contains PbI_2 (613.14 mg mL⁻¹), FAI (228.72 mg mL⁻¹), PbBr₂ (25.69 mg mL⁻¹), MABr (7.84 mg mL⁻¹), and MACl (33.08 mg mL⁻¹) using DMF/DMSO mixed solvent (the volume ratio of DMF to DMSO is 8:1) to obtain 0.5 M (FAPbI₃)_{0.95}(MAPbBr₃)_{0.05}. The devices were fabricated on the patterned ITO/glass substrates described above. The substrates were cleaned in air sequentially with soapy water, deionized water, acetone, and isopropyl alcohol, and were then dried by N_2 and treated with O_2 plasma for 10 min prior to film deposition in an N_2 -filled glovebox. PTAA (5 mg mL⁻¹ in chlorobenzene) with the F_4 TCNQ dopant (0.2 mg mL⁻¹ in chlorobenzene) was then spin-coated at 1500 rpm for 60 s andthermally annealed at 110 °C for 20 min. The samples were then treated with O_2 plasma for 15 s to improve wettability for the subsequent perovskite layer, which was spin-coated initially at 1,000 rpm for 10 s (with an acceleration rate of 200 rpm/s), and then 5,000 rpm for 30 s (with an acceleration rate of 2000 rpm/s). A solvent-

quenching step was performed 20 s after spinning by dropping chlorobenzene (0.2 mL) on the spinning samples. The samples were then annealed at 100 °C for 30 min and loaded into a thermal evaporator to deposit 10 nm of undoped PO-T2T followed by 30 nm of PO-T2T doped with [RuCp*Mes]₂ in a 5:1 volume ratio via co-evaporation. The device was completed by depositing a 100 nm-thick Ag cathode through a shadow mask.

Characterization. At the start of testing, devices were illuminated with a Xe arc lamp for 20 min at room temperature to activate doping by [RuCp*Mes]₂²⁰ in the cryostat prior to lowering the temperature. Devices were measured within 8 h of this step. Most measurements of a given device were completed within one hour, though this sometimes extended to 4 h for streak camera measurements. Because of the small device size and collection spot, the temperature in the cryostat had to stabilize completely so that thermal expansion/contraction of the cold finger did not move the device under study by more than 1 µm in 30 min relative to the microscope. Following thermal stabilization, one device was selected for a sacrificial measurement in order to establish the upper bound on electrical pulse amplitude that could be tolerated before the onset of degradation. As long as the electrical pulses were kept within the limit determined from the sacrificial device, no degradation was observed over the course of testing on the other devices, consistent with previous high current pulsing measurements.⁵ The repetition rate of all optical and electrical pulses was 20 Hz. Full details of the synchronization and timing setup are provided in the Supplementary Material.

Acknowledgement

The authors acknowledge support for this work from DARPA Award No. N66001-20-1-4052 and the Eric and Wendy Schmidt Transformative Technology Fund. A.J.G. and J.P.M. acknowledge support from the National Research Council, Research Associateship Program. L.Z. and K.A./S.B./S.R.M. acknowledge support from the National Science Foundation under Award Nos. ECCS-2304364 and DMR-1807797/2216857, respectively.

Supporting Information Available

The Supporting Information is available free of charge on the ACS Publications website at DOI: XXXXXXX.

Details of the electrical pulsing circuit, simulations of the DFB threshold optical gain, and LED co-pumping measurements using 3 ns pulses.

References

- (1) Gunnarsson, W. B.; Roh, K.; Zhao, L.; Murphy, J. P.; Grede, A. J.; Giebink, N. C.; Rand, B. P. Toward Nonepitaxial Laser Diodes. *Chem. Rev.* **2023**, *123*, 7548–7584.
- (2) Jia, Y.; Kerner, R. A.; Grede, A. J.; Rand, B. P.; Giebink, N. C. Continuous-Wave Lasing in an Organic-Inorganic Lead Halide Perovskite Semiconductor. *Nat. Photonics* 2017, 11, 784.
- (3) Brenner, P.; Bar-On, O.; Jakoby, M.; Allegro, I.; Richards, B. S.; Paetzold, U. W.; Howard, I. A.; Scheuer, J.; Lemmer, U. Continuous Wave Amplified Spontaneous Emission in Phase-Stable Lead Halide Perovskites. *Nat Commun* **2019**, *10*, 988.
- (4) Roh, K.; Zhao, L.; Rand, B. P. Tuning Laser Threshold within the Large Optical Gain Bandwidth of Halide Perovskite Thin Films. *ACS Photonics* **2021**, *8*, 2548–2554.
- (5) Zhao, L.; Roh, K.; Kacmoli, S.; Al Kurdi, K.; Liu, X.; Barlow, S.; Marder, S. R.; Gmachl, C.; Rand, B. P. Nanosecond-Pulsed Perovskite Light-Emitting Diodes at High Current Density. Advanced Materials 2021, 33, 2104867.
- (6) Kim, H.; Zhao, L.; Price, J. S.; Grede, A. J.; Roh, K.; Brigeman, A. N.; Lopez, M.; Rand, B. P.; Giebink, N. C. Hybrid Perovskite Light Emitting Diodes under Intense Electrical Excitation. *Nat. Commun.* 2018, 9, 1–9.

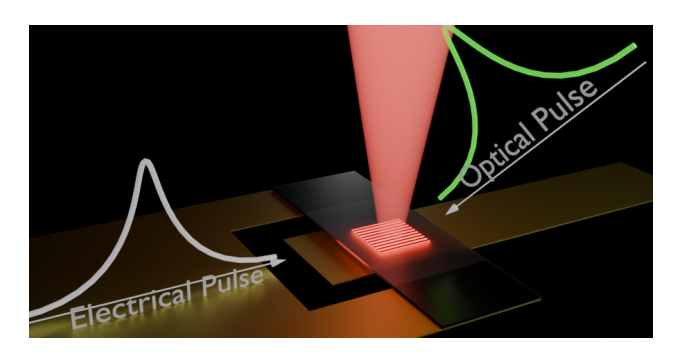
- (7) Elkhouly, K.; Goldberg, I.; Annavarapu, N.; Gehlhaar, R.; Ke, T.-H.; Genoe, J.; Hofkens, J.; Heremans, P.; Qiu, W. Intense Electrical Pulsing of Perovskite Light Emitting Diodes under Cryogenic Conditions. *Adv. Opt. Mater.* **2022**, *10*, 2200024.
- (8) Zou, C.; Liu, Y.; Ginger, D. S.; Lin, L. Y. Suppressing Efficiency Roll-Off at High Current Densities for Ultra-Bright Green Perovskite Light-Emitting Diodes. ACS Nano 2020, 14, 6076–6086.
- (9) Elkhouly, K.; Goldberg, I.; Zhang, X.; Annavarapu, N.; Hamdad, S.; Croes, G.; Rolin, C.; Genoe, J.; Qiu, W.; Gehlhaar, R.; Heremans, P. Electrically Assisted Amplified Spontaneous Emission in Perovskite Light-Emitting Diodes. *Nat. Photon.* 2024, 18, 132–138.
- (10) Zhao, L.; Roh, K.; Kacmoli, S.; Al Kurdi, K.; Jhulki, S.; Barlow, S.; Marder, S. R.; Gmachl, C.; Rand, B. P. Thermal Management Enables Bright and Stable Perovskite Light-Emitting Diodes. Adv. Mater. 2020, 32, 2000752.
- (11) deQuilettes, D. W.; Frohna, K.; Emin, D.; Kirchartz, T.; Bulovic, V.; Ginger, D. S.; Stranks, S. D. Charge-Carrier Recombination in Halide Perovskites. *Chem. Rev.* 2019, 119, 11007–11019.
- (12) Jia, Y.; Kerner, R. A.; Grede, A. J.; Rand, B. P.; Giebink, N. C. Factors That Limit Continuous-Wave Lasing in Hybrid Perovskite Semiconductors. Adv. Opt. Mater. 2020, 8, 1901514.
- (13) Li, Y.; Hu, H.; Farag, A.; Feeney, T.; Allegro, I.; Lemmer, U.; Paetzold, U. W.; Howard, I. A. Enhancement of Amplified Spontaneous Emission by Electric Field in CsPbBr3 Perovskites. *Nano Lett.* 2023, 23, 1637–1644.
- (14) Chime, A. C.; Bensmida, S.; Chakaroun, M.; Lee, M. W.; Nkwawo, H.; Fischer, A. P. A. Electrical Modelling and Design of Ultra-Fast Micro-OLED with Coplanar Wave-Guided Electrodes in ON-OFF Regime. Org. Electron. 2018, 56, 284–290.

- (15) Zhang, Q.; Shang, Q.; Su, R.; Do, T. T. H.; Xiong, Q. Halide Perovskite Semiconductor Lasers: Materials, Cavity Design, and Low Threshold. *Nano Lett.* **2021**, *21*, 1903–1914.
- (16) Zhu, H.; Fu, Y.; Meng, F.; Wu, X.; Gong, Z.; Ding, Q.; Gustafsson, M. V.; Trinh, M. T.; Jin, S.; Zhu, X.-Y. Lead Halide Perovskite Nanowire Lasers with Low Lasing Thresholds and High Quality Factors. *Nature Mater* **2015**, *14*, 636–642.
- (17) Pourdavoud, N.; Wang, S.; Mayer, A.; Hu, T.; Chen, Y.; Marianovich, A.; Kowalsky, W.; Heiderhoff, R.; Scheer, H.-C.; Riedl, T. Photonic Nanostructures Patterned by Thermal Nanoimprint Directly into Organo-Metal Halide Perovskites. *Adv. Mater.* **2017**, *29*, 1605003.
- (18) Karnutsch, C.; Pflumm, C.; Heliotis, G.; deMello, J. C.; Bradley, D. D. C.; Wang, J.; Weimann, T.; Haug, V.; Gärtner, C.; Lemmer, U. Improved Organic Semiconductor Lasers Based on a Mixed-Order Distributed Feedback Resonator Design. Applied Physics Letters 2007, 90, 131104.
- (19) Un, H.-I.; Gregory, S. A.; Mohapatra, S. K.; Xiong, M.; Longhi, E.; Lu, Y.; Rigin, S.; Jhulki, S.; Yang, C.-Y.; Timofeeva, T. V.; Wang, J.-Y.; Yee, S. K.; Barlow, S.; Marder, S. R.; Pei, J. Understanding the Effects of Molecular Dopant on N-Type Organic Thermoelectric Properties. Adv. Energy Mater. 2019, 9, 1900817.
- (20) Lin, X.; Wegner, B.; Lee, K. M.; Fusella, M. A.; Zhang, F.; Moudgil, K.; Rand, B. P.; Barlow, S.; Marder, S. R.; Koch, N.; Kahn, A. Beating the Thermodynamic Limit with Photo-Activation of n-Doping in Organic Semiconductors. *Nature Mater* 2017, 16, 1209–1215.

For Table of Contents Use Only

Title: Electrically-assisted lasing in metal halide perovskite semiconductors

Authors: Alex Grede, Robert Cawthorn, Lianfeng Zhao, John Murphy, Kwangdong Roh, Khaled Al Kurdi, Stephen Barlow, Seth Marder, Barry Rand, Noel Giebink



Synopsis: Illustration of a surface-emitting metal halide perovskite laser diode (red rectangle) under combined electrical (left, gray) and optical (right, green) excitation. The optically-pumped threshold of the device decreases when the electrical and optical pulses overlap, demonstrating that electrical injection contributes appreciably to lasing.